Millimeter-Wave Enhanced Local Area Systems: A High-Data-Rate Approach for Future Wireless Networks

Amitava Ghosh, *Senior Member, IEEE*, Timothy A. Thomas, *Member, IEEE*, Mark C. Cudak, *Member, IEEE*, Rapeepat Ratasuk, Prakash Moorut, *Member, IEEE*, Frederick W. Vook, *Senior Member, IEEE*, Theodore S. Rappaport, *Fellow, IEEE*, George R. MacCartney, Jr., *Student Member, IEEE*, Shu Sun, *Student Member, IEEE*, and Shuai Nie, *Student Member, IEEE*

***Abstract*—Wireless data traffic is projected to skyrocket 10 000 fold within the next 20 years. To tackle this incredible increase in wireless data traffic, a first approach is to further improve spectrally efficient systems such as 4G LTE in bands below 6 GHz by using more advanced spectral efficiency techniques. However, the required substantial increase in system complexity along with fundamental limits on hardware implementation and channel conditions may limit the viability of this approach. Furthermore, the end result would be an extremely spectrally efficient system with little room for future improvement to meet the ever-growing wireless data usage. The second approach is to move up in frequency, into an unused nontraditional spectrum where enormous bandwidths are available, such as at millimeter wave (mmWave). The mmWave option enables the use of simple air interfaces since large bandwidths can be exploited (e.g., 2 GHz) to achieve high data rates rather than relying on highly complex techniques originally aimed at achieving a high spectral efficiency with smaller bandwidths. In addition, mmWave systems will easily evolve to even higher system capacities, because there will be plenty of margin to improve the spectral efficiency as data demands further increase. In this paper, a case is made for using mmWave for a fifth generation (5G) wireless system for ultradense networks by presenting an overview of enhanced local area (eLA) technology at mmWave with emphasis on 5G requirements, spectrum considerations, propagation and channel modeling, air-interface and multiantenna design, and network architecture solutions.**

***Index Terms*—mmWave, 5G, enhanced local area, spectrum, propagation, channel modeling, air-interface design, modulation.**

I. Introduction

WIRELESS data traffic is projected to increase by 1000 fold by the year 2020 [1] and is likely to grow by more than 10 000 fold by the year 2030 [2]. To meet this incredible projected increase in traffic demand, the throughput per square meter in wireless networks must be increased by either shrinking cell sizes (with associated interference mitigation), greatly increasing spectral efficiency, acquiring additional spectrum, or doing some combination of these three. In other words, the 10 000 fold increase in network capacity could be achieved through an increase in performance, spectrum availability and massive densification of small cells as illustrated in Fig. 1.

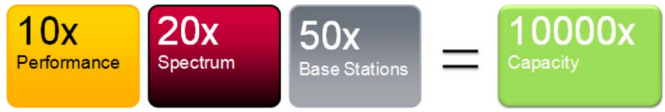

Fig. 1. Achieving 10 000× capacity.

There are two obvious methods which can be attempted in addition to massive cell densification to meet this needed large increase in capacity. The first approach is to do everything possible to increase the throughput of LTE systems [3] below 6 GHz using massive MIMO, carrier aggregation, coordinated multipoint, heterogeneous networks, authorized shared access and any number of interference management/cancellation techniques. However, all of these methods at the very best may only meet the 1000 fold increase, but will not be able to grow much beyond that point given high spectral efficiency already obtained with MIMO (e.g., up to 8 × 8 MIMO in LTE), interference management techniques, and the limited spectrum available. The second option is to move to new frequency bands, which have a tremendous amount of spectrum, and to exploit large bandwidths to achieve very high peak and cell edge rates. Particular bands of interest are the millimeter-wave (mmWave) bands of 20–90 GHz and more specifically the 28 and 38 GHz bands (where there is 3–4 GHz available) and the 70 and 80 GHz E-band where there is an incredible 10 GHz of spectrum available, as shown in Fig. 2. The E-band is of particular interest over other mmWave bands because it is already lightly licensed and is provisioned to allow up to 5 GHz of contiguous bandwidths. Introducing fifth generation (5G) in the E-band would require a new set of rules, but reusing the currently allowed channel bandwidth could facilitate the introduction of 5G in this band from a regulatory point of view.

In this paper, we explore the use of the mmWave band (20–100 GHz) to design the 5G enhanced local area (eLA) access which satisfies the requirements for 5G networks with

Manuscript received December 1, 2013 ; revised April 25, 2014; accepted May 25, 2014. Date of publication June 3, 2014; date of current version July 14, 2014.

A. Ghosh, T. A. Thomas, M. C. Cudak, R. Ratasuk, P. Moorut, and F. W. Vook are with Nokia, Arlington Heights, IL 60004 USA (e-mail: timothy.thomas@nsn.com).

T. S. Rappaport, G. R. MacCartney Jr., S. Sun, and S. Nie are with the NYU WIRELESS Research Center in the Department of Electrical and Computer Engineering, NYU Polytechnic School of Engineering, Brooklyn, NY 11201 USA.

Color versions of one or more of the figures in this paper are available online at http://ieeexplore.ieee.org.

Digital Object Identifier 10.1109/JSAC.2014.2328111

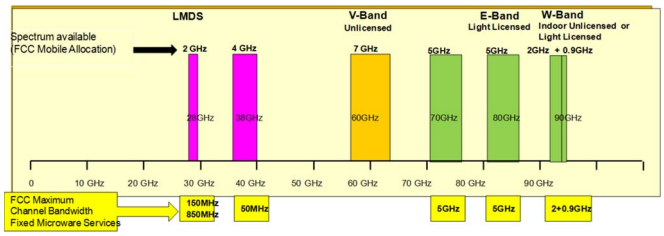

Fig. 2. Some potential 5G spectrum above 20 GHz.

peak rates in excess of 10 Gbps, cell-edge rates of at least 100 Mbps, and latencies of less than 1.0 msec. The availability of huge bandwidth coupled with the use of large antenna arrays with as many as 8 to 256 elements (9 to 24 dB in link budget gain) at both transmitter and receiver can make this band attractive for deploying high capacity 5G networks. Note that such high gain antennas can be implemented in tiny, flexible form factors, much less than a few square centimeters for use on cell phones of the future, due to the extremely small wavelength at mmWave frequencies [4]–[7]. Furthermore, the unique propagation conditions at mmWave necessitate some fundamental changes to the system. Hence, new system concepts and procedures must be defined to effectively utilize this new spectrum resource. The 5G networks will also offer superior user experience by providing sub-millisecond latency, gigabits-per-second speed and improved energy efficiency. In addition, the networks will be self-aware, self-adaptable and intelligent.

This paper is organized as follows. Section II discusses spectrum and regulatory issues for 5G mmWave communications. In Section III, propagation characteristics and channel modeling aspects for mmWave bands are discussed using recent channel measurements in New York City. Section IV proposes a modulation strategy based on the null cyclic-prefix single-carrier concept. Section V proposes a network architecture and frame structure that are both designed to satisfy the requirements and the unique propagation characteristics at mmWave frequency bands. Section VI presents system simulation results showing the performance of an example 5G eLA system deployed at mmWave. Finally, conclusions are drawn in Section VII.

II. Spectrum and Regulatory Issues

To date, the cellular industry has mostly focused on obtaining additional spectrum below 6 GHz. In particular, in the USA, approximately 2.27 GHz of potential new spectrum was identified by NTIA and the National Broadband Plan [8] where approximately 550 MHz is expected to be made available to the cellular industry in the next five years. However, what has been neglected is the enormous 94 GHz of spectrum from 6 to 100 GHz. Even if only a fraction (say 1/3) of that spectrum were to be made available to the cellular industry, that would amount to around 31 GHz of new spectrum, which is significantly higher than the spectrum available below 6 GHz. By providing more spectra for future mmWave cellular systems, the future capacity demands could be met, while simultaneously incentivizing investments and technological developments that would ensure engineering competitiveness. Fig. 2 highlights the bands in this region with the highest potential, and we discuss each in more detail below.

- **28 GHz band (27.5–29.5 GHz range)** [9]: The 27.5–28.35 GHz (850 MHz) and 29.1–29.25 GHz (150 MHz) portions of this band operate under FCC Part 101 rules for Fixed Microwave Services. These two sub-bands are called the Local Multipoint Distribution Service (LMDS) band in the USA. Other services in this band include FSS (Fixed Satellite Service), GSO (Geostationary Orbit), NON-LTTS (Non-Local Television Transmission Service), MSS (Mobile Satellite Service), and NGSO (Non-Geostationary Orbit).
- **38 GHz band (36–40 GHz)**: The 38.6–40 GHz portion of this band operates under FCC Part 101 rules for Fixed Microwave Services and is used for fixed point-to-point microwave operations that provide backhaul links.
- **57–64 GHz band (V-band or 60 GHz band)**: Currently this band is provisioned for unlicensed operation as per FCC Part 15.255 regulations. This band does have a large amount of oxygen absorption (see the next section) but it does not significantly hamper communications especially for small cells (e.g., distances of less than around 200 m). These frequencies may not be the first choice for a cellular mmWave system since 802.11ad is designed to be used in this band and also due to the unlicensed nature of this band.
- **71–76 GHz and 81–86 GHz (E-band or the 70 GHz and 80 GHz bands, respectively)**: This band operates under a lightly licensed paradigm as per FCC Part 101 and there are no limits in aggregating this band up to a total of 2×5 GHz. At this band the oxygen absorption is much less of an issue than at 60 GHz. Rain attenuation can be severe with longer distances but will not be a problem for small distances such as less than around 200 m.
- **92–95 GHz band (W-band or 90 GHz band)**: This band is provisioned for unlicensed operation but only for indoor applications, as per FCC Part 15.257. Except for an excluded radio-astronomy band at 94–94.1 GHz, this band can be used for outdoor point-to-point licensed-light operation per FCC Part 101 regulations.

Hence, the 28 GHz, 38 GHz, 71–76 GHz and 81–86 GHz bands are excellent candidates for deploying 5G local area networks mostly due to the 16 GHz of available bandwidth and channel bandwidth currently available. However, 10 GHz is available in the 71–76 and 81–86 GHz bands with up to 5 GHz of contiguous bandwidth available making these bands appear most attractive for a mmWave system. Note, however, that any 5G system operating in the 71–86 GHz bands must coexist with fixed satellite service, automotive radar (77–81 GHz), and radio astronomy.

Although we used the US FCC regulations as examples, these bands are also available in many countries. All of the bands have a mobile allocation in the ITU-R Radio Regulations. Note also that other countries have similar spectrum allocations in the 28 and 38 GHz bands, and the 60 GHz band is a global unlicensed band with different subsets of 57–66 GHz available in Europe, USA, Canada, Japan, Korea, Australia, and China.

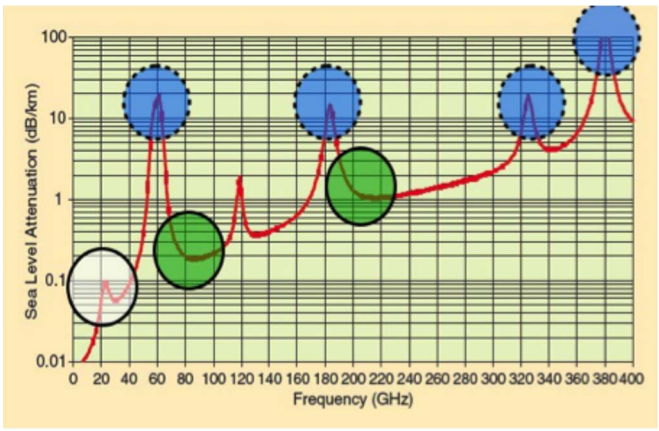

Fig. 3. Air attenuation at microwave and mmWave frequency bands [4].

The 70 GHz and 80 GHz E-bands are available in Europe under a license-light regime similar to the USA.

III. Propagation Characteristics and Channel Modeling

Millimeter waves have been largely dismissed for cellular communications, due to their perceived higher atmospheric and rain attenuation properties from the early days of satellites, but Fig. 3 shows that atmospheric attenuation in urban microcells is virtually negligible. Specifically, for small cells with 200 m radii, atmospheric attenuation is approximately 0.06 dB/km and 0.08 dB/km at 28 GHz and 38 GHz, respectively, and is about 0.3 dB/km at frequencies between 70 and 90 GHz. Since urban microcells will be designed for inter-site distances within 200 meters (both for backhaul and access), air attenuation will be of little concern. Similarly, rain attenuation is much less severe over distances of 200 meters, even during extremely heavy rain events, providing at most 3 to 6 dB of attenuation in the very worst rain conditions, and much less during heavy rain events [4], [5], [10]. Researchers at NYU WIRELESS conducted a wideband propagation measurement campaign in the summer of 2012 in New York City at 28 GHz and showed that mmWaves will work for future generations of wireless [5].

Recent wideband measurement campaigns in New York City and Brooklyn, NY at 28 GHz and 73 GHz (RF at 73.5 GHz) [10], [11] have verified that large contiguous bandwidths in the mmWave bands are viable for both backhaul and access for 5G. The researchers used a sliding correlator channel sounding system similar to that used in [5], [12]. The 400 Mega-chip per second (Mcps) spread spectrum sliding correlator channel sounder was developed to measure the 73 GHz radio channel by transmitting a spread spectrum pseudorandom code centered around 73.5 GHz with an ultrawide 800 MHz first null-to-null RF bandwidth. The channel sounding system records power delay profiles (PDPs) that can provide up to 2.5 nanosecond multipath time resolution, and highly directional rotatable horn antennas were used at both the TX (transmitter) and RX (receiver).

The 73 GHz measurements were conducted in downtown New York City around NYU's campus, which offers a very rich multipath environment. Measurements consisted

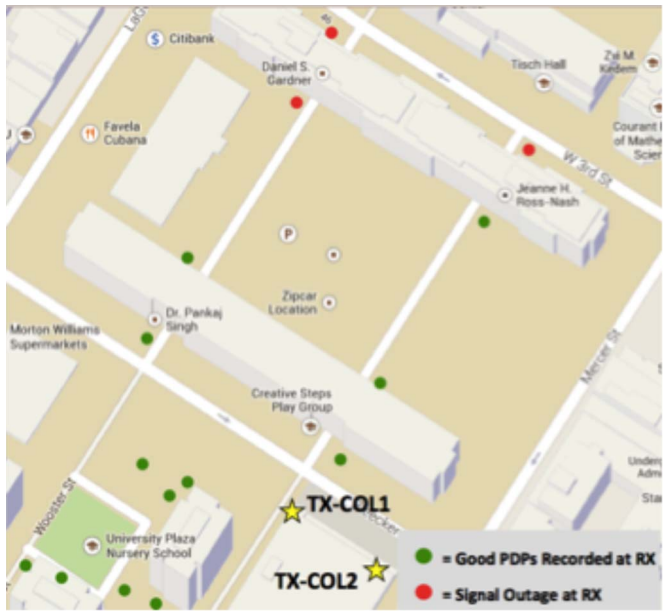

Fig. 4. Map of TX and RX measurement locations around NYU's campus. TX locations for Coles Sports Center are yellow stars and are at heights of 7 meters. The RX locations are represented as green and red circles.

of both backhaul-to-backhaul and base-station-to-access scenarios, with TX and RX inter-site distances between 30 and 200 meters. Two TX locations were on top of NYU's Coles Sports Center at heights of 7 meters, two TX locations were on the 2nd floor balcony of the Kimmel Center at heights of 7 meters, a final TX location was on the 5th floor balcony of the Kaufman building at a height of 17 meters, and 27 RX locations were located in the surrounding campus at heights of 2 meters (access) and 4.06 meters (backhaul). Fig. 4 shows the measurement locations. A majority of the measurements were in non line-of-sight (NLOS) conditions, as LOS conditions are less common in dense-urban environments. Also, RX locations were pseudo-randomly selected around the campus based on AC outlet access and prior NYU Public Safety approval.

The TX and RX antennas used for the 73 GHz measurements were rotatable 27 dBi horn antennas with a 7° 3 dB-beamwidth. Information regarding the entire hardware setup and detailed measurement configurations can be found in [11], [12]. The NYU WIRELESS research team conducted measurements for 36 base station-to-access and 38 backhaul-to-backhaul combinations, however, there were outages at various locations for each scenario.

The measurements at 73 GHz show very comparable path loss behavior for the base station-to-access scenarios measured at 28 and 38 GHz [5], [7], [10], thus indicating that mmWave propagation in many different bands will be quite comparable and quite viable with directional, high gain antennas used at both the mobile device and base station.

In this work, we have created the first published omni-directional large-scale path loss models at 73 GHz for backhaul and mobile access in an urban environment. These new omni-directional path loss models are suitable for use by standards bodies and academicians who may wish to study arbitrary antenna patterns or MIMO approaches. The omni-directional

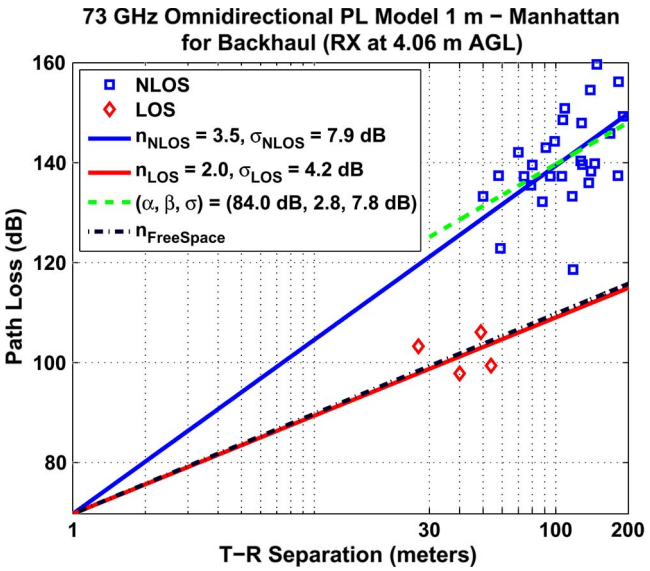

Fig. 5. Measured omni-directional path loss computed relative to 1 m free space path loss for 73 GHz backhaul-to-backhaul (TX height was 17 m and 7 m and the RX height was 4.06 m). Note that a popular 3GPP-style alpha plus beta omni-directional path loss model [14] over the range of 30–200 m is also shown on the graphs.

path loss models were created by considering the measured PDPs at every individual and unique pointing angle for each TX and RX location combination, and integrating each of the PDPs to obtain received power as a function of pointing angle, and then subtracting the TX and RX antenna gains from every individual power measurement. We then summed up all of the received powers at unique pointing angles (taking care not to double count for replicated antenna pointing angles) to obtain the omni-directional path loss models given here. Results of the 73 GHz omni-directional measurements from New York City are shown in Fig. 5, where best fit path loss exponents (PLEs) are shown for the omni-directional backhaul-to-backhaul scenario. Path loss and shadow factors (i.e., the standard deviation about the distance-dependent mean path loss model) were computed for both LOS and NLOS measurements for each scenario. Two path loss models are considered in this paper. The first model, the free space path loss (FSPL) reference distance model, provides a path loss exponent which has physical relevance since the path loss is tied to the FSPL at a specific close-in reference distance (1 m is convenient and practical at mmWave frequencies). In equation form, this path loss is given by:

$$PL[dB](d) = 20\log_{10}\left(\frac{4\pi d_0}{\lambda}\right) + 10\bar{n}\log_{10}\left(\frac{d}{d_0}\right) + X_\sigma \quad (1)$$

where d_0 is the reference distance (1 m in this paper), λ is the wavelength, $\bar{n}$ is the path loss exponent, d is the distance between TX and RX in m, and X_σ is the shadow fading term which is a zero-mean Gaussian variable with a given standard deviation, σ (i.e., the shadow fading) in dB. For the large-scale propagation model in (1), the path loss exponent and shadow fading standard deviation are chosen to give the best fit to the data. The second path loss equation considered is the traditional

TABLE I
PATH LOSS EXPONENTS (RELATIVE TO A FREE SPACE REFERENCE DISTANCE OF 1 m) AND SHADOW FACTORS FOR THE FSPL REFERENCE DISTANCE MODEL FOR NEW YORK CITY AT 73 GHz WITH TX HEIGHTS OF 17 m AND 7 m WITH BACKHAUL-TO-BACKHAUL RX HEIGHTS OF 4.06 m, AND BASE STATION-TO-ACCESS SCENARIOS WITH RX HEIGHTS OF 2 m. PLEs AND SHADOW FACTORS ARE SHOWN FOR OMNI-DIRECTIONAL ANTENNAS AT THE RX AND TX

	73 GHz Backhaul-to-Backhaul		73 GHz Base Station-to-Access	
	PLE	**SF (dB)**	**PLE**	**SF (dB)**
LOS	2.0	4.2	2.0	5.2
NLOS	3.5	7.9	3.3	7.6

TABLE II
ALPHA, BETA, AND SHADOW FACTORS FOR THE ALPHA PLUS BETA MODEL FOR NEW YORK CITY AT 73 GHz WITH TX HEIGHTS OF 17 m AND 7 m WITH BACKHAUL-TO-BACKHAUL RX HEIGHTS OF 4.06 m, AND BASE STATION-TO-ACCESS SCENARIOS WITH RX HEIGHTS OF 2 m. α, β, AND SHADOW FACTOR PARAMETERS ARE SHOWN FOR OMNI-DIRECTIONAL ANTENNAS AT THE RX AND TX. ALSO SHOWN IS A HYBRID MODEL SIMILAR TO THAT IN [14] THAT CONSIDERS BOTH BACKHAUL AND ACCESS MEASUREMENTS FOR THE MODEL (RX HEIGHTS OF 2 m AND 4.06 m).

	NLOS Floating Intercept Models		
	α **(dB)**	β	**SF (dB)**
Backhaul-to-Backhaul	84.0	2.8	7.8
Base Station-to-Access	81.9	2.7	7.5
Hybrid	80.6	2.9	7.8

one used in industry (e.g., by 3GPP) and we will refer to it as an *alpha plus beta* model. This model has the following form:

$$PL[dB](d) = \alpha + 10\beta\log_{10}(d) + X_\sigma \quad (2)$$

where α and β are determined with a least squares fit to the measured data and X_σ is the shadow fading term. Note that this path loss formula is limited to only the range of distances measured in the field [13]. In (2), β cannot be considered to be a true path loss exponent because it is floating and is only chosen to optimize the fit to the data along with the y-intercept, α. Also, since the path loss formula in (2) is only valid over the range for which the measurements were taken, it is inaccurate and often misleading for distances where the physical model of (1) will still hold [13], [14]. The advantage of the *alpha plus beta* model is that it minimizes the standard deviation (minimizes the mean square error fit to data) with an improvement of about 0.5 to 1 dB to a FSPL model, but the disadvantage is that there is no physical basis for the model and it does not fit real world data well beyond the specific range of data for which it is created.

Fig. 5 shows that the measured omni-directional LOS path loss is very close to the free space path loss for the backhaul case. Also shown is how the *alpha plus beta* model compares to the FSPL reference distance model. Over the range of distances of the measured data (30 to 200 m in [14]), both models produce similar path loss values, but outside of that range the two models would deviate quite significantly. Table I summarizes the results found for the omni-directional 1 m FSPL reference distance model for the scenarios of both backhaul-to-backhaul and base station-to-access, and Table II summarizes the path loss models for the *alpha plus beta* model. These results show

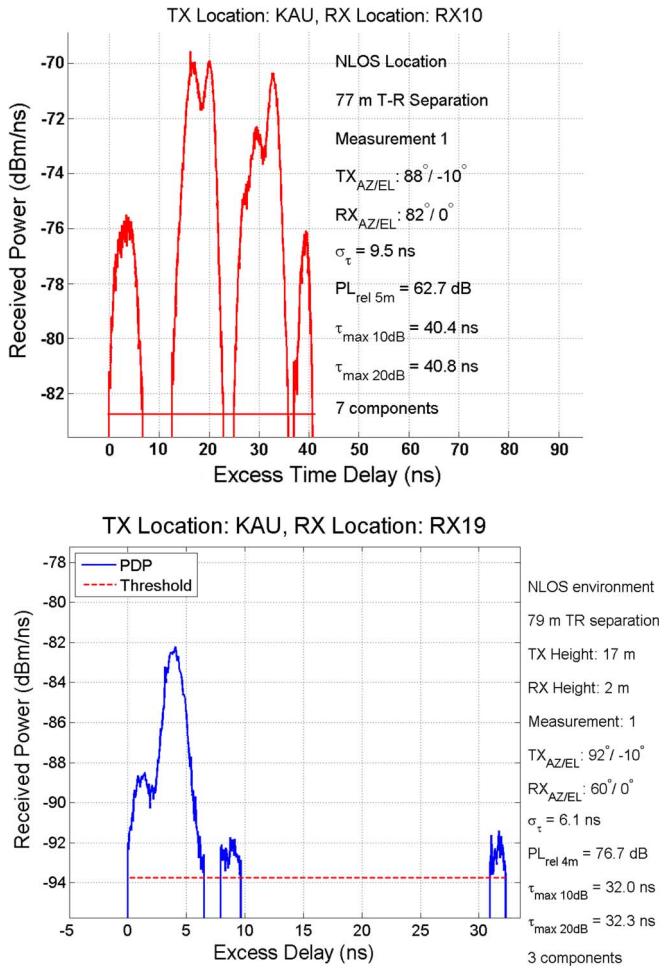

Fig. 6. Two PDPs measured in nearly identical locations in New York City (one year apart) at 28 GHz (top) [15] and 73 GHz [11] (bottom). The 28 GHz PDP has slightly larger multipath delay spread and more resolvable multipath components, probably due to smaller surface roughness of the reflectors at the lower frequency band.

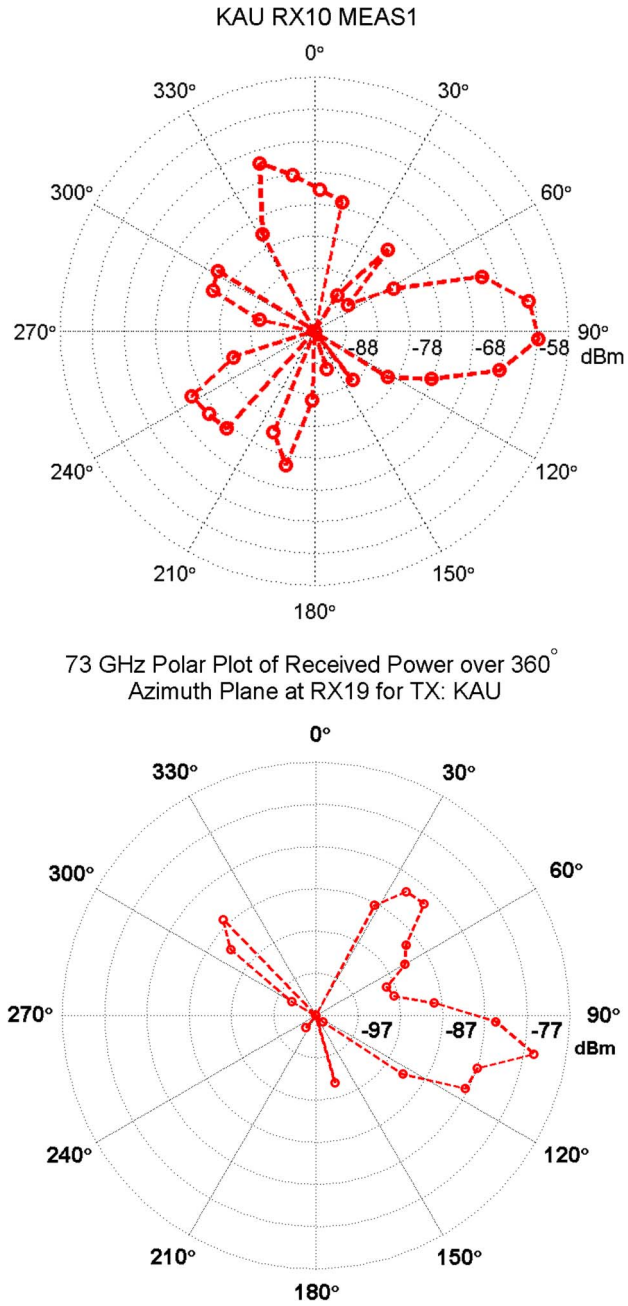

Fig. 7. Two polar plots measured at similar locations at 28 GHz (top) [15] and 73 GHz (bottom) [11] (one year apart). These plots show the different Angles of Arrival (AOAs) on the azimuthal plane at 28 GHz and 73 GHz in a NLOS environment. Note that the TX directions of departure were slightly different for the measurements used to generate these plots. Zero degrees refers to when the RX antenna is facing true north.

that the omni-directional NLOS PLEs for the backhaul-to-backhaul and base station-to-access scenarios are comparable to one another, and are also quite comparable to urban path loss observed at 28 GHz [14], [15].

These recent mmWave measurements in New York City show that the propagation channel is rich in multipath, both in terms of time delays and angular arrivals. This diversity provides ample signal paths that will be exploited to provide multi-Gigabit per second data transmissions in the vast mmWave spectrum bands [16]. Fig. 6 shows typical measured PDPs that have a large number of strong multipath components when using highly directional antennas at the TX and RX. Fig. 7 compares the angles of arrival at 28 and 73 GHz, and it shows that distinctive lobes of energy arrive in a similar manner at a wide array of different angles in the environment.

In order to develop statistical channel models to enable the standardization of mmWave wireless technologies, extensive and careful measurements, data processing, and simulation tools must be developed for the nascent mmWave wireless industry. Early work aimed at creating standards for channel models is underway. For example, Fig. 7 suggests that multipath lobes may be used to statistically describe the arrival of energy when using directional antennas, where the lobe size may be a function of the particular antenna gain used at the receiver [15]. Early path loss, multipath, and RMS delay spread models have appeared in the literature for mmWave channels, and more measurements and data processing will be required by the academic community to better understand the new opportunities provided by mmWave spectrum [4], [5], [7], [10]–[13], [17].

Path loss and time/angle spread models for determining coverage and outage expectations for future 5G mmWave systems are needed for a wide range of frequencies, and early work has provided possible models for determining coverage

and capacity at mmWave frequencies in both the 28 and 73 GHz bands, and for mobile access and backhaul channels [10], [11], [13], [15]. NYU WIRELESS researchers continue to mine the 200 Gigabytes of measured propagation data from 2012 and 2013 measurement campaigns to create models that can be used by academia and industry to implement modems that will exploit high gain antennas and the new mmWave propagation channel.

IV. Modulation Proposal for 5G mmWave

Given the popularity of orthogonal frequency division multiplexing (OFDM) in 4G cellular, one would think that OFDM would be a natural choice for mmWave communications. However, an important feature of OFDM for use below 6 GHz, the multiplexing of users in frequency, is not necessarily a valuable feature for the much wider bandwidths at mmWave. There are many reasons why this feature may not be important for mmWave communications. First, mmWave will be deployed in small cells with very small slot sizes (e.g., 100 μsec), meaning very few users will need to transmit within a slot. Second, the high bandwidth and small cell coverage results in small OFDM symbol times (e.g., 66.67 μsec) and small propagation delays, meaning that the active users could just as efficiently be multiplexed in time, rather than frequency. Lastly, mmWave systems will need large antenna arrays at least at one end of the link to overcome path loss. Full digital beamforming will be impractical at least initially since the digital to analog converters (D/As) and analog to digital converters (A/Ds) that are needed behind each of the antennas and operate at 2.0 GHz bandwidths will consume an unacceptable amount of power. This drives initial mmWave systems to use RF beamforming which requires only a single A/D and D/A behind the entire array of antennas. The use of RF beamforming implies that only a single beam per polarization can be created at any given time, thus necessitating users to be separated in time, rather than frequency, since each user will use a unique beam which provides the best gain for that user.

Since the ability to multiplex users in frequency is not critical for mmWave access communications, it therefore may not be necessary to accept some of the drawbacks of OFDM, such as the high peak to average power ratio (PAPR) which inefficiently operates the power amplifiers (PAs) thus shrinking the expected range and also can negatively impact out-of-band emissions. Thus we propose using a form of cyclic prefix (CP) single carrier (SC) modulation, and in particular, suggest replacing the regular CPs with null CPs. This concept is called null CP SC (NCP-SC) [18] and has near-constant-envelope properties and is inherently efficient such as LTEs 4G reverse link [3] which uses DFT-spread OFDM (DFT-S-OFDM).

For both OFDM and single carrier modulation, a cyclic prefix is the repetition of the last N_{CP} symbols in an FFT block and enables efficient frequency-domain equalization by turning time-domain linear convolution with a channel into circular convolution. The idea is to create a CP-SC signal but with nulls replacing the usual CPs. As shown in Fig. 8 we propose appending N_{CP} null symbols at the end of a block of N symbols where the null symbols of one block are effectively the

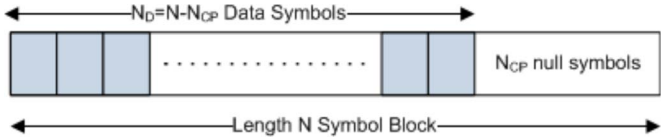

Fig. 8. NCP-SC symbol.

CP for next block of symbols. The number of data symbols is given by $N_D = N - N_{CP}$, and note that the size of the symbol block, N, is the same regardless of the CP size. As a result, the CP length can be adaptively changed on a per-user basis without altering the frame timing simply by puncturing the data. The frequency-domain receiver will then operate by taking an oversampled FFT (e.g., a $2N$ point FFT) of the appropriate received block of N symbols. Note that we chose to use a null CP system instead of the training-prefix system of 802.11ad [19] which instead of null symbols uses the same known training symbols as CPs on each block. The advantages of using the null CP over the training prefixes will be enumerated below.

Note that compared to NCP-SC, OFDM has a lower computational complexity in the transmitter and receiver. The reason is that OFDM just needs a single IFFT at the transmitter and a single FFT at the receiver. For NCP-SC both an FFT and an IFFT are needed at the receiver, and either the transmitter needs to implement a fairly computationally intensive time-domain pulse filtering or the pulse shaping must be performed in the frequency-domain requiring both an FFT and an IFFT. Note, however, other aspects such as coding and decoding of the data will be similar between OFDM and NCP-SC, and it is possible that the complexity of the coding could dominate the computational complexity given the high data rates of these mmWave systems. However, the following advantages of NCP-SC still make NCP-SC the preferred choice at mmWave frequencies (these advantages hold over both OFDM and DFT-S-OFDM):

1) The null cyclic prefixes provide a dead time for ramping down and ramping up beams steered at RF, so that the RF beams can be changed in between NCP-SC symbols without destroying the cyclic prefix property nor requiring additional guard time. This makes switching users within a slot very efficient.
2) The null cyclic prefix is actually part of the NCP-SC symbol which is FFT'd into the frequency domain (as opposed to being appended in the case of OFDM). This has the desirable feature of keeping the FFT size the same regardless of the null cyclic prefix size. This feature enables the system to dynamically change the cyclic prefix size per-user without changing the overall slot and frame sizes/lengths.
3) The null CP provides an easy way to estimate post-equalizer noise plus interference (i.e., in the null portion of the symbol, no desired signal energy should be present).
4) As will be described next, NCP-SC has much lower PAPR and better out-of-band emissions than OFDM.

Note that NCP-SC has three out of the four advantages just mentioned as compared to 802.11ad's single carrier approach [19] which has a similar structure to NCP-SC shown in Fig. 8

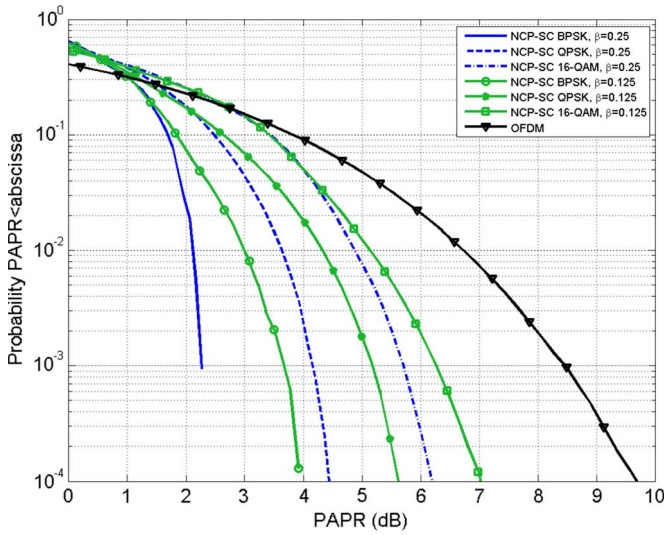

Fig. 9. PAPR of NCP-SC compared to OFDM.

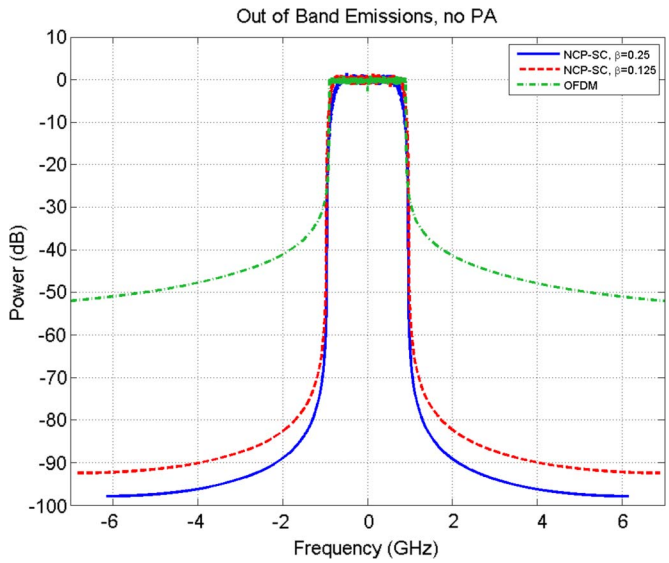

Fig. 10. Out of band emissions of NCP-SC compared to OFDM.

with the exception that 448 data symbols are present and the null symbols are replaced with 64 known pilot symbols which are a length-64 Golay sequence. Hence the only common advantage that could be maintained by 802.11ad's single carrier option is number 2 where the CP length could change dynamically if multiple training prefix lengths were defined by 802.11ad. Note that the abrupt transition from data to the training symbols would increase the PAPR and degrade the out-of-band emissions relative to NCP-SC. It should also be noted that the training prefixes would enable coherent tracking of unknown phase offsets (e.g., caused by large frequency offset errors or from severe phase noise) from one symbol block to the next, but the same can be done in NCP-SC with blind techniques [20] reliably since there are a large number of data symbols available to perform the blind carrier offset tracking.

Fig. 9 shows the PAPR benefit of NCP-SC compared to OFDM for different roll-off factors used in the root-raised cosine pulse of NCP-SC. Besides the PAPR benefits of NCP-SC over OFDM, there is also a benefit in out-of-band emissions as shown in Fig. 10. The abrupt transmissions between two adjacent OFDM symbols creates much higher out-of-band emissions than NCP-SC where the transitions go to zero between different symbol blocks. Thus NCP-SC will have a much easier time meeting spectral masks especially for interference created in adjacent bands which are currently used for things such as automotive radar. It should also be noted that there will be PAPR benefits over DFT-S-OFDM as well but they will be less than the improvements over OFDM.

Finally the performance of NCP-SC versus OFDM should be considered. Here OFDM has an advantage when using traditional cellular frequencies in macro cells (read large cell distances) with small antenna arrays at each end. For this case the channel is likely Rayleigh faded with many channel taps meaning the frequency-domain channel exhibits many nulls. Since the equalization of NCP-SC is generally MMSE, these nulls can reduce the performance compared to OFDM which can take advantage of ML equalization. However in mmWave, the channel tends to be very Ricean because the use of large

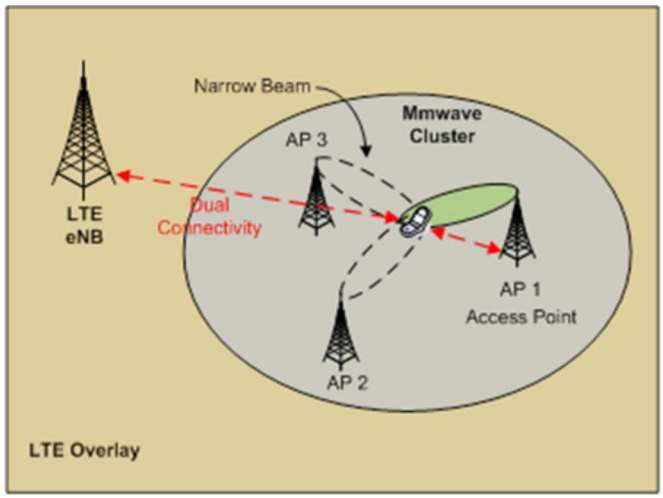

Fig. 11. mmWave cluster with LTE overlay.

arrays tends to filter out most of the multipath, and with small cell sizes (expected inter-site distances less than 200 m) the channels will mostly be LOS, near LOS, or consist of a single reflected path. In Ricean channels the benefits of the ML equalization of OFDM evaporate as we have seen in expected mmWave channels.

V. 5G eLA Network Architecture and Air Interface

Here we discuss a high level architecture for future 5G deployments. As shown earlier, high shadowing loss and outages occur at certain antenna pointing angles, thus particular access points may not be able to achieve a radio link with certain users, depending on particular antenna configurations or locations. As a result, a set or cluster of cooperating access points (APs) may be deployed to cover an area, as shown in Fig. 11. A user may therefore be covered by multiple access points within the cluster, such that the shadowed areas are covered from a unique propagation direction through appropriate access point placement.

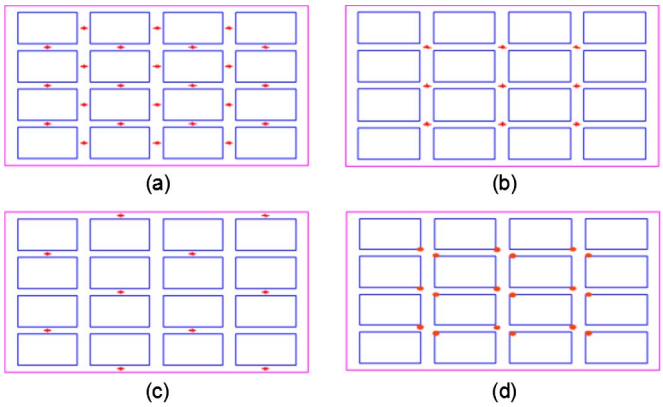

Fig. 12. Deployment options for cooperating clusters. (a) Mid-block deployment; (b) intersection deployment; (c) sparse mid-block deployment; (d) dense staggered deployment.

Fig. 11 also illustrates mmWave access point deployment with an LTE overlay to provide dual connectivity to both systems. With dual connectivity, the user can be simultaneously connected to both the LTE overlay and to one or more mmWave access points. In this way, the radio link can always be maintained should access to the mmWave clusters become unavailable. This approach can also be used to maximize the user experience by combining the high data rate of the mmWave system with the reliability of the LTE overlay. For instance, control-plane transmission can be sent via LTE to ensure continuous radio link while user-plane transmission can be sent on either LTE or mmWave.

To maximize mmWave coverage and minimize outage, overlapping deployment strategies should be considered to enhance the effectiveness of the cooperating cluster. Consider the regular Manhattan grid depicted in Fig. 12. The figure shows four options for mmWave base station deployment where base stations are illustrated with red asterisks; buildings—which are effectively opaque at mmWave—are shown as blue boxes and street coverage is depicted as the area between the blue boxes. Conventional deployments for small cells are depicted in (a) intersection deployment and (b) mid-block deployment. These same deployments could be re-used for mmWave clusters as there is reasonable overlap between adjacent serving cells. Option (c) shows a sparse mid-block deployment that, while potentially useful for 4G cellular, would not be effective at mmWave because the coverage areas of adjacent cells would have little overlap region and would rely on LOS from the primary serving cell which could suffer from shadowing loss. Option (d) shows a dense staggered deployment and is a good example of what would be required for mmWave deployments. In this case, base stations are deployed on opposite street corners and the base station pairs provide a diversity effect reducing the probability of shadowing and improving the coverage reliability. Cars, trucks, trees and people which might block the LOS to a base station on one side of the street would be unlikely to block the base station on the opposing side of the street. The dense staggered deployment is one example of how to improve mmWave coverage reliability to the levels enjoyed by conventional cellular.

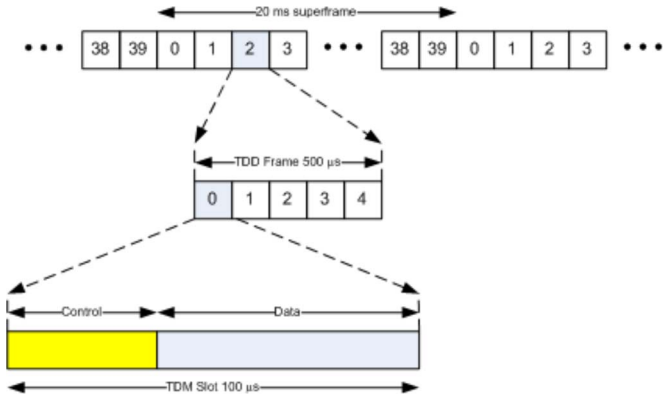

Fig. 13. TDD frame structure.

In addition to the network architecture just described, an important requirement of the 5G eLA system will be to achieve a significant reduction in the latency of the air interface. The frame structure of the system can be designed to meet a 1 msec latency requirement. In particular, a super frame (e.g., 20 msec) could be broken up into subframes (e.g., 500 microseconds in length), and a subframe would contain some number of slots (e.g., 5 slots of length 100 microseconds) as shown in Fig. 13. The 5G system will be targeted towards TDD operation, and each subframe could either be uplink, downlink, or backhaul, and can be configured differently from access point to access point (this technique is referred to as dynamic TDD). The small subframe length makes meeting the 1 msec latency easy, and the use of TDD, and in particular, dynamic TDD, makes the 5G system very flexible and bandwidth and power efficient. Additional details of a proposed mmWave 5G system can be found in [18].

VI. 5G eLA Performance

This section summarizes the system-level results with a brief comparison to the scenarios defined by METIS [21]. An urban street environment is simulated as shown in Fig. 14 with three different densities of APs being employed where all APs are 5 m high. The first scenario has 36 APs which are located on the street corners (5 m east and 5 m south of the northwest building corner) as given by the green pluses in the figures. The second scenario has 72 APs with two APs at the intersection of two streets but with the APs at opposite street corners (the green pluses and blue dots) with the additional APs from scenario 1 being 5 m west and 5 m north of the southeast building corner. The third scenario has 96 APs located in the middle of street blocks (5 m from the buildings) and at street corners (the green pluses and the red circles). Note that the blocking probabilities of the channel between a user equipment (UE, aka mobile) and two APs are independent regardless of how close the APs are to each other. This means that scenario 2 will have a significant advantage over scenario 1 in that the blocking probability to a UE will be greatly reduced. LOS blocking is modeled in two ways where the first is where the squares in the figure model street blocks (which may be a single or multiple buildings) where the LOS signal is completely blocked if these squares are between a UE and an AP. The second LOS blocking is a random

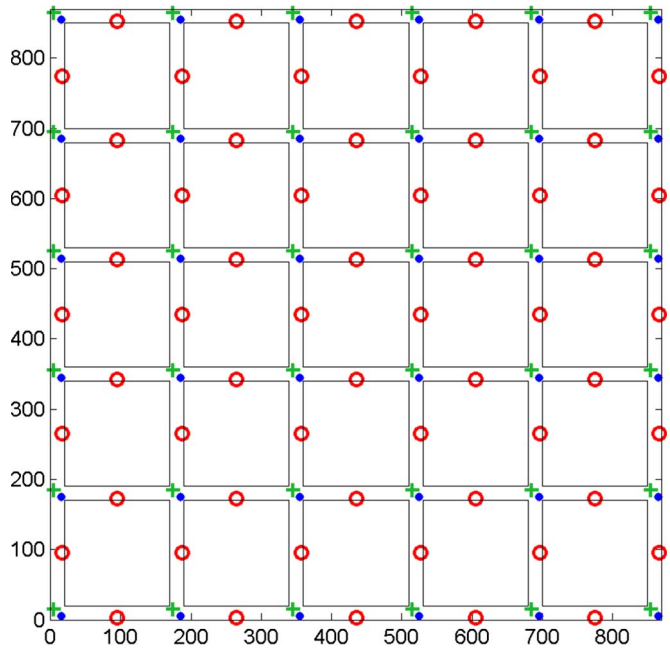

Fig. 14. Layout of the APs for an urban-street environment. APs for first scenario are green +, for the second scenario are green + and blue dots, for the third scenario are green + and red circles. The black squares represent city blocks consisting of multiple buildings which block the mmWave signal.

blocking given by the following distance-dependent blocking probability:

$$P_{block} = \min(0.0078d + 0.1, 0.8), \tag{3}$$

where d is the 2D distance (i.e., distance in the x-y plane) between AP and UE in meters. This model for blocking probability was generated through ray tracing where various blocking objects such as cars, trucks, trees, and pedestrians are randomly placed in the environment. Complete details of this blocking probability model can be found in [22].

When no blocking is present (neither the random blocking nor the building blocking), a LOS path loss was used and is given by (d is in meters and log means base-ten log)

$$PL[dB](d) = 69.6 + 20.9\log(d) + X_\sigma \tag{4}$$

with a shadow fading of 5.0 dB. In the case of blocking the channel was considered NLOS with a path loss given at 72 GHz by

$$PL[dB](d) = 69.6 + 33\log(d) + X_\sigma \tag{5}$$

with a shadow fading of 7.6 dB. Note that these path loss formulas match the reference distance model in (1) and Table I for access models, except that the LOS shadow fading value was 5.0 and the path loss exponent was 2.09 where both values were based on previous calculations which where subsequently refined. These slight differences should not significantly impact the simulation results nor conclusions drawn from them.

The scenarios considered here are not too dissimilar than the urban environmental model of METIS [21]. A first difference between models is that METIS defines a 4×3 grid of city blocks instead of our 5×5 grid of city blocks. The next difference between the two models is that METIS repeats their 4×3 grid to create a wrap-around effect whereas our scenario was exactly as shown. We simply exclude UEs dropped along the outer 75 m of the scenario from the system statistics. METIS also defines a very complex user dropping which may include higher densities near street intersections, a random movement of users, and a higher user density along sidewalks. Our users were static and uniformly dropped along the streets. The METIS environment may also have parks, bus stops, and dual-stripe buildings (instead of a continuous building in the block).

TABLE III
SYSTEM SIMULATION PARAMETERS

Parameter	Value
Bandwidth and CF	CF:72 GHz, BW: 2.0 GHz
Symbol rate	1.536 GHz (50x LTE)
Traffic type	Full buffer, 100 users/drop, 10 drops
AP array	4 sectors, each sector has two 4x4 arrays (one vertically polarized one horizontally polarized) with 0.5 spacing in both dimensions
Mobile antennas	2 omni antennas, one with vertical polarization, other with horizontal polarization
AP Tx power	30.8 dBm/sector (split between the two arrays in each sector)
Maximum rank	2
Beamforming	Eigen beamforming using the uplink signal
Modulation levels	LTE MCS levels
Channel estimation	Ideal
Scheduler	Proportional fair

The channel model details are given in [23] but a brief summary is now given. The channel is derived from both the NYU measurements and a ray tracer for the same environment as the NYU measurements which was tuned to give path loss results similar to the measured results. The channel model is a 3GPP-style ray-based model which includes distant-dependent elevation angle spreads for the urban-micro environment. The model includes both LOS and NLOS versions with the blocking probability plus building blocking being used to determine NLOS links.

The system-level parameters are given in Table III. Each AP consists of 4 sectors with each sector having two 4×4 arrays, one with horizontal polarization and the other with vertical polarization (two polarizations are employed to enable two-stream SU-MIMO along with single-stream transmission). The UE has two co-located omni-directional antennas each with a different polarization (either horizontal or vertical). Thus with RF beamforming the two stream MIMO channel looks like a 2×2 channel at the UE with each stream being sent from a different RF beam where the beams are chosen by doing Eigen beamforming across all transmit antennas. The LTE modulation and coding rates are employed. Full buffer traffic is assumed and proportional fair scheduling is employed. The transmit power is 30.8 dBm in each sector (shared between both arrays in the sector). In the simulations no hybrid automatic repeat request (HARQ) procedures were employed since the

TABLE IV
SYSTEM SIMULATION RESULTS (MINIMUM THROUGHPUT IS THE MINIMUM THROUGHPUT OF UEs NOT IN OUTAGE DEFINED BY A THROUGHPUT OF LESS THAN 100 Mbps)

Parameters	Scenario 1	Scenario 2	Scenario 3
Ave. UE throughput	3.2 Gbps	5.6 Gbps	6.5 Gbps
Cell edge throughput	0 Mbps	26.7 Mbps	461 Mbps
Max. throughput	15.7 Gbps	15.7 Gbps	15.7 Gbps
Min. throughput	0 Mbps	0 Mbps	0 Mbps
Outage probability	19.7%	5.98%	3.15%

TABLE V
SYSTEM SIMULATION RESULTS FOR SCENARIO 1 WITH A 4×4 AND AN 8×8 ARRAY

Parameters	4x4	8x8
Ave. UE throughput	3.2 Gbps	4.86 Gbps
Cell edge throughput	0 Mbps	0 Mbps
Max. throughput	15.7 Gbps	15.7 Gbps
Min. throughput	0 Mbps	0 Mbps
Outage probability	19.7%	11.5%

assumption is that link adaptation should be excellent given the Ricean nature of the beamformed channel and that the links being predominantly noise limited. However, retransmissions are allowed.

The simulation results comparing the scenarios are summarized in Table IV. Scenario 1 is hampered by a relatively large distance between APs and hence when all channel rays are blocked it is difficult for the UE to attach to the next AP. This effect is seen by the relatively large outage probability of 19.7% (an outage is defined as a UE throughput of less than 100 Mbps). However, scenario 1 still sees a very impressive 3.2 Gbps average UE throughput however with a disappointing 0 Mbps cell edge rate (cell edge is defined as the 5% UE throughput). However by adding just a single AP at the opposite street corner as in scenario 2 the outage probability drops substantially to around 5.98%. The drop is attributed to having another AP relatively nearby which can be connected to if the channel to the closest AP is completely blocked. In addition the average UE throughput improves to 5.6 Gbps and the cell edge throughput improves to 26.7 Mbps for scenario 2. Further increasing the AP density as in scenario 3 gives further improvements in cell average UE throughput to 6.5 Gbps and a cell edge throughput to 461 Mbps while decreasing the outage to 3.15%.

Besides increasing AP density, increasing the array size at the AP can also greatly improve the blocking probability and system-level performance. Consider Table V which shows a comparison of the system-level results for two 4×4 arrays per sector to two 8×8 arrays per AP sector for scenario 1. The blocking probability of the 8×8 arrays drops to around 11.5% which is good but it still is not enough to overcome blockage and hence AP densification is needed. The average UE throughput increases by quite a bit to around 4.86 Gbps, but the cell edge throughput is still a disappointing 0 Mbps indicating that further AP densification is needed (or antenna arrays are needed at the UE).

VII. CONCLUSION

In this article, a case is made for using mmWave bands, in particular the 28, 38, 71–76 and 81–86 GHz bands for a 5G eLA. Extensive channel measurements show very comparable path loss behavior for both the access and backhaul scenarios for 28 and 73 GHz bands in New York City. This indicates that mmWave propagation in many different bands will be quite comparable and viable for eLA deployment with directional, high gain antennas used at the mobile device and access points. The mmWave systems achieve similar coverage at different bands since for the same form factor larger antenna arrays can be used at high bands to compensate for the path loss difference between high and low mmWave bands. The eLA system described in this paper exploits large bandwidths in the mmWave regime to achieve peak data rates in excess of 10 Gbps and edge data rates of more than 100 Mbps. We proposed null cyclic prefix single carrier modulation for mmWave systems and presented simulation results showing the system-level performance of the proposed eLA system can achieve cell edge rates in excess of 100 Mbps with proper densification of the access points.

ACKNOWLEDGMENT

The authors would like to acknowledge NYU WIRELESS students Rimma Mayzus, Hannar J. Lee, and Abhi Shah who supported the Summer 2013 73 GHz measurements in New York City, as well as the NYU Department of Public Safety, and the New York Police Department. The authors also appreciate the support of the NYU WIRELESS industrial affiliate companies and the National Science Foundation. Measurements were recorded under U.S. FCC Experimental License 0040-EX-ML-2012.

REFERENCES

[1] B. Raaf *et al.*, "Vision for beyond 4G broadband radio systems," in *Proc. IEEE 22nd Int. Symp. PIMRC*, Sep. 2011, pp. 2369–2373.
[2] T. S. Rappaport *et al.*, "Special session on mmWave communications," in *Proc. ICC*, Budapest, Hungary, Jun. 2013.
[3] 3rd Generation Partnership Project (3GPP), "Evolved Universal Terrestrial Radio Access (E-UTRA); Physical channels and modulation (Release 8)," Sophia-Antipolis, France, TS 36.201, 2009, (R9-2010, R10-2010, R11-2012).
[4] T. S. Rappaport, J. Murdock, and F. Gutierrez, "State of the art in 60-GHz integrated circuits and systems for wireless communications," *Proc. IEEE*, vol. 99, no. 8, pp. 1390–1436, Aug. 2011.
[5] T. S. Rappaport *et al.*, "Millimeter wave mobile communications for 5G cellular: It will work!" *IEEE Access*, vol. 1, pp. 335–349, 2013.
[6] F. Gutierrez, S. Agarwal, K. Parrish, and T. Rappaport, "On-chip integrated antenna structures in CMOS for 60 GHz WPAN systems," *IEEE J. Sel. Areas Commun.*, vol. 27, no. 8, pp. 1367–1378, Oct. 2009.
[7] T. S. Rappaport *et al.*, "Broadband millimeter-wave propagation measurements and models using adaptive-beam antennas for outdoor urban cellular communications," *IEEE Trans. Antennas Propag.*, vol. 61, no. 4, pp. 1850–1859, Apr. 2013.
[8] G. Locke and L. E. Strickling, "Plan and timetable to make available 500 megahertz of spectrum for wireless broadband," U.S. Department of Commerce, Washington, D.C., USA, Oct. 2010.
[9] FCC 28 & 31 GHz Band Plan. [Online]. Available: http://wireless.fcc.gov/auctions/data/bandplans/lmds.pdf
[10] Y. Azar *et al.*, "28 GHz propagation measurements for outdoor cellular communications using steerable beam antennas in New York City," in *Proc. IEEE ICC*, Jun. 2013, pp. 5143–5147.

[11] G. R. MacCartney and T. S. Rappaport, "73 GHz millimeter wave propagation measurements for outdoor urban mobile and backhaul communications in New York City," in *Proc. IEEE ICC*, Jun. 2014.
[12] S. Nie, G. R. MacCartney, S. Sun, and T. S. Rappaport, "72 GHz millimeter wave indoor measurements for wireless and backhaul communications," in *Proc. IEEE 24th Int. Symp. PIMRC*, Sep. 2013, pp. 2429–2433.
[13] G. R. MacCartney, J. Zhang, S. Nie, and T. S. Rappaport, "Path loss models for 5G millimeter wave propagation channels in urban microcells," in *Proc. IEEE GLOBECOM*, Dec. 2013, pp. 1–6.
[14] S. Rangan, T. S. Rappaport, and E. Erkip, "Millimeter-wave cellular wireless networks: Potentials and challenges," *Proc. IEEE*, vol. 102, no. 3, pp. 366–385, Mar. 2014.
[15] M. Samimi *et al.*, "28 GHz angle of arrival and angle of departure analysis for outdoor cellular communications using steerable beam antennas in New York City," in *Proc. IEEE 77th VTC-Spring*, Jun. 2013, pp. 1–6.
[16] M. R. Akdeniz, Y. Liu, S. Rangan, and E. Erkip, Millimeter Wave Picocellular System Evaluation for Urban Deployments, Apr. 15, 2013, arXiv preprint arXiv:1304.3963 (also see *IEEE ICC 2013, and IEEE Communications Theory Workshop*, June 2013).
[17] S. Sun and T. S. Rappaport, "Multi-beam antenna combining for 28 GHz cellular link improvement in urban environments," in *Proc. IEEE GLOBECOM*, Dec. 2013, pp. 1–6.
[18] M. Cudak *et al.*, "Moving towards mmwave-based beyond-4G (b-4G) technology," in *Proc. IEEE 77th VTC-Spring*, Jun. 2013, pp. 1–5.
[19] *IEEE Draft Standard for Local and Metropolitan Area Networks—Specific Requirements—Part 11: Wireless LAN Medium Access Control (MAC) and Physical Layer (PHY) Specifications—Amendment 3: Enhancements for Very High Throughput in the 60 GHz band*, IEEE P802.11ad/D5, 2011.
[20] F. Rice, B. Cowley, B. Moran, and M. Rice, "Cramer–Rao lower bounds for QAM phase and frequency estimation," *IEEE Trans. Commun.*, vol. 49, no. 9, pp. 1582–1591, Sep. 2001.
[21] Simulation Guidelines, Deliverable D6.1, METIS document number ICT-317669-METIS/D6.1, Oct. 31, 2013.
[22] T. A. Thomas and F. W. Vook, "System level modeling and performance of an outdoor mmWave local area access system," *IEEE PIMRC*, to be published.
[23] T. A. Thomas, H. C. Nguyen, G. R. MacCartney, Jr., and T. S. Rappaport, "3D mmWave Channel Model Proposal," in *Proc. IEEE VTC-Fall*, 2013, pp. 1–6.

Amitava Ghosh (SM'97) received the Ph.D. degree in electrical engineering from Southern Methodist University, Dallas, TX, USA. In 1990, he joined Motorola, where he has been working on multiple wireless technologies starting from IS-95, cdma-2000, 1xEV-DV/1XTREME, 1xEV-DO, UMTS, HSPA, 802.16e/WiMAX/802.16m, Enhanced EDGE, and 3GPP LTE. Currently, he is the Head of the North American Radio Systems Research Group, Technology and Innovation Office, Nokia, Arlington Heights, IL, USA. He is currently working on 3GPP LTE-Advanced and 5G technologies. He is a coauthor of the book titled *Essentials of LTE and LTE-A*. He has 60 issued patents and numerous external and internal technical papers. His research interests are in the areas of digital communications, signal processing, and wireless communications.

Timothy A. Thomas (M'97) received the B.S. degree in electrical engineering from the University of Illinois at Urbana-Champaign, Urbana, IL, USA, in 1989; the M.S. degree in electrical engineering from the University of Michigan, Ann Arbor, MI, USA, in 1990; and the Ph.D. degree in electrical engineering from Purdue University, West Lafayette, IN, USA, in 1997. From 1991 to 1993, he was a member of the Technical Staff at Bell Communications Research (Bellcore), Red Bank, NJ, USA, and from 1997 to 2011, he was with Motorola, Schaumburg, IL, working on wireless research. Since 2011, he has been with the North American Radio Systems Research Group, Technology and Innovation Office, Nokia, Arlington Heights, IL. His research interests are in physical-layer communications and particularly channel measurements, cellular and millimeter-wave communications, and adaptive antenna algorithms for mobile broadband communications.

Mark C. Cudak (M'90) received the M.S. degree in electrical engineering from the University of Illinois at Urbana-Champaign, Urbana, IL, USA. He is currently a Principal Research Specialist with the North American Radio Systems Research Group, Technology and Innovation Office, Nokia, Arlington Heights, IL. Prior to joining Nokia, he was with Motorola for 20 years where he worked on a variety of wireless data systems, including GPRS, WCDMA, HSPA, WiMAX, and LTE. He has more than 40 issued patents. His research is focused on cellular network evolution looking at how 4G and 5G radio advances can be applied to real-world networks.

Rapeepat Ratasuk received the Ph.D. degree in electrical engineering from Northwestern University, Evanston, IL, USA, in 2000. He is currently a Principal Research Specialist with the North American Radio Systems Research Group, Technology and Innovation Office, Nokia, Arlington Heights, IL. He has an extensive experience in 3G/4G cellular system design and analysis, including algorithm development, performance analysis and validation, physical-layer modeling, and simulations. He is a coauthor of the book titled *Essentials of LTE and LTE-A*. He has more than 35 issued patents and more than 40 journal and conference papers. His current research interests are in the areas of wireless and machine-to-machine communications.

Prakash Moorut received the M.S.E.E. degree from the École Supérieure d'Electricité (SUPELEC), Gif-Sur-Yvette, France. He is currently the North America Spectrum Lead of Nokia, Arlington Heights, IL, USA. In this role, he is responsible for working with regulators, operators, and industry members to open more useable commercial mobile broadband spectrum in North America. He has more than 17 years of experience working in Europe and USA on numerous wireless technologies and is currently enabling small cells, 5G technologies, and spectrum sharing. Before joining Nokia, he was with Motorola where he created and led a customer-facing spectrum engineering group located in USA, France, and China. He has several publications and patents related to spectrum usage.

Frederick W. Vook (SM'04) received the B.S. degree from Syracuse University, Syracuse, NY, USA, in 1987 and the M.S. and Ph.D. degrees from The Ohio State University, Columbus, OH, USA, in 1989 and 1992, respectively, all in electrical engineering. From 1992 to 1995, he was with the Motorola Wireless Data Group where he worked on 19- and 2.4-GHz propagation modeling and air interface design for Motorola's wireless LAN products. From 1995 to 2008, he was with Motorola Laboratories, where he worked on MIMO, beamforming, and air interface design for broadband mobile communication systems. From 2008 to 2011, he was with Motorola Home & Networks Mobility where he worked on physical-layer modeling and MIMO techniques for IEEE 802.16/WiMAX and LTE Rel-8-10. Since 2011, he has been with the North American Radio Systems Research Group, Technology and Innovation Office, Nokia, Arlington Heights, IL, USA, where his current work involves advanced antenna array solutions for LTE and 5G cellular systems. He has more than 50 issued patents with another 20 patents pending.

Theodore S. Rappaport (S'83–M'84–SM'91–F'98) is the David Lee/Ernst Weber Professor of Electrical and Computer Engineering with New York University (NYU) Polytechnic School of Engineering, Brooklyn, NY, USA, and is the Founding Director of NYU WIRELESS. He also holds professorship positions with Courant Institute of Mathematical Sciences and the School of Medicine, NYU. He founded major wireless research centers at Virginia Polytechnic Institute and State University, The University of Texas at Austin, and NYU, and founded two wireless technology companies that were sold to publicly traded firms. He is a highly sought-after Technical Consultant having testified before the U.S. Congress and having served the ITU. He has advised more than 100 students, has more than 100 patents issued and pending, and has authored or coauthored several book, including the best-seller *Wireless Communications: Principles and Practice*, Second Edition (Prentice Hall, 2002). His latest book, *Millimeter Wave Wireless Communications* (Pearson/Prentice Hall), is the first comprehensive text on the subject.

George R. MacCartney Jr. (S'08) received the B.S. and M.S. degrees in electrical engineering from Villanova University, Villanova, PA, USA, in 2010 and 2011, respectively. He is currently working toward the Ph.D. degree in electrical engineering with New York University Polytechnic School of Engineering, Brooklyn, NY, USA, with Prof. T. Rappaport, focused on millimeter-wave propagation and modeling for 5G communication systems. Since January 2013, he has been with NYU WIRELESS, New York University Polytechnic School of Engineering.

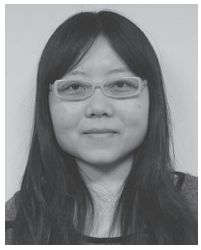

Shu Sun (S'13) received the B.S. degree in applied physics from Shanghai Jiao Tong University, Shanghai, China, in 2012. She is currently working toward the Ph.D. degree in electrical engineering with New York University Polytechnic School of Engineering (NYUPoly), Brooklyn, NY, USA. Since August 2012, she has been with NYU WIRELESS, NYUPoly. She has coauthored two conference publications and is now working on millimeter-wave (mmWave) propagation measurements campaign for 5G cellular mmWave communication systems.

Shuai Nie (S'13) received the M.S. degree in electrical and computer engineering from New York University Polytechnic School of Engineering, Brooklyn, NY, USA, in 2014. Since January 2013, she has been with NYU WIRELESS, New York University Polytechnic School of Engineering. She has coauthored four conference publications and is now working on the effect of vegetation on millimeter-wave propagation and system coverage studies.